

The MSSM-30 in light of the $B_s \rightarrow \mu^+ \mu^-$ observation

S.S. AbdusSalam^{1(a)} and L. Velasco-Sevilla^{2(b)}

^(a) Department of Physics, Shahid Beheshti University, Tehran 19839, Islamic Republic of Iran

^(b) University of Bergen, Department of Physics and Technology, POB 7803, 5020 Bergen, Norway

Abstract

The R-parity conserving MSSM in light of the decay $B_s \rightarrow \mu^+ \mu^-$ with near-SM branching ratio is an interesting platform for studying the complementarity between direct and indirect searches for beyond the SM physics. Based on this, we have analysed the possible impact of the $B_s \rightarrow \mu^+ \mu^-$ observation on the MSSM pseudo-scalar Higgs boson mass, m_A and the related Wilson coefficients. A 15% relative error in the measurement of the branching ratio, compared to the current 20% error, will indicate that m_A must be in the sub-TeV region. This is done within a systematically, symmetry-guided, constructed 30-parameter MSSM (MSSM-30) in contrast to the traditional frames (e.g. pMSSM) with crude treatment of flavour violation parameters. This paper illustrates why phenomenological frames like the MSSM-30 should be preferred to study flavour physics. For the current and future B-physics experimental precision, such a consideration is crucial for suitably assessing supersymmetric contributions to flavour observables.

¹Email: abdussalam@sbu.ac.ir

²Email: Liliana.Velasco-Sevilla@ift.uib.no

Contents

1	Introduction	1
2	The MSSM-30 parameters in light of the $B_s \rightarrow \mu^+ \mu^-$ observation	3
2.1	The MSSM-30 frame	3
2.2	$\text{BR}(B_s \rightarrow \mu^+ \mu^-)$ prediction and measurement	4
3	MSSM-30 contributions to $B_s \rightarrow \mu^+ \mu^-$	7
3.1	Diagram-by-diagram and particle-by-particle contributions	9
3.2	Contributions to C_P and C_S	9
3.3	Contributions to C_{10}	13
3.4	Interplay of Wilson coefficients	15
3.5	Interplay of off-diagonal soft-squared elements	16
4	Conclusions	18

1 Introduction

The decay $B_s \rightarrow \ell^+ \ell^-$ has been used traditionally as indicator of how contributions from extended Higgs sectors, with respect to the Standard Model (SM), can give sizeable contributions to leptonic decays and semi-leptonic decays. This happens because its branching fraction undergoes a helicity suppression by $m_\mu^2/M_{B_s}^2$, where m_μ is the mass of the muon and M_{B_s} is the mass of the B_s meson. This suppression can be lifted in models with extra Higgs doublets [1, 2]. Hence, these decays provide a good opportunity to look after physics beyond the Standard Model (BSM). For the particular BSM case of the R-parity conserving minimal supersymmetric standard model (MSSM), with diagonal soft-squared mass matrices and trilinear terms, analytical approximations indicate that the $B_s \rightarrow \mu^+ \mu^-$ decay amplitude can be proportional to $\tan^3 \beta$ [3, 4, 5, 6, 7]. $\tan \beta$ is the the ratio of the MSSM Higgs fields vacuum expectation values $\langle H_2 \rangle / \langle H_1 \rangle$ which can take values between 2 and 60. However, full-fledged (numerical) analyses including global fits of models to data have shown that BSM contributions to $B_s \rightarrow \mu^+ \mu^-$ behave in a multi-dimensional manner.

The various contributions are mostly suppressed with respect to the SM one or have opposite signs with similar magnitudes. Examples showing the manifestation of this was shown within the phenomenological MSSM (pMSSM) frame [8, 9], where the $\text{BR}(B_s \rightarrow \mu^+ \mu^-)$ posterior distribution lies around the Standard Model (SM) prediction despite the moderately high values of $\tan \beta$, and in the more recent work of [10].

While the observation of $B_s \rightarrow \mu^+ \mu^-$ by the LHCb and CMS experiments ruled out the possibility of having large deviations of $\text{BR}(B_s \rightarrow \mu^+ \mu^-)$ from the SM prediction [11, 12, 13, 14, 15, 16, 17, 18], the $\text{BR}(B_s \rightarrow \mu^+ \mu^-)$ alone is not sensitive enough for limiting all the huge MSSM parameter space. However, it is an interesting observable which is well capable of constraining the pseudoscalar mass, m_A , as a function of the value of $\tan \beta$. Within the plane m_A versus $\tan \beta$, the sensitivity to the branching ratio of the decay $B_s \rightarrow \mu^+ \mu^-$ is complementary, or it can have competing effects, to direct searches for new physics.

The target of this paper is as follows. We would like to draw inference on the MSSM parameter space based on a robust numerical anatomy of the MSSM contributions to the $\text{BR}(B_s \rightarrow \mu^+ \mu^-)$.

Given the amazing consistency of the predictions of the SM with flavor observables one may wonder if in supersymmetry there is a mechanism behind, such that just as it happens in the SM, it effectively forbids flavor changing processes (FCNC) and controls CP violation. Specific models with a MSSM spectrum which avoid FCNC and CP violating processes can be constructed successfully [30, 31, 32]. However, without an specific model for generation of flavour within the MSSM, it is imperative to work within a phenomenological frame with a systematically constructed parametrisation of flavour violation. Following this rationale, we consider a MSSM frame with 30 parameters [20, 21] which goes beyond the constrained MSSM(s) (see [22, 23, 24, 25, 26, 27, 28] for related works within the constrained MSSM(s) frames) and the pMSSM [29, 33, 8] where flavour violation in the SUSY breaking mass terms is manipulated by hand albeit with reasonable motivations.

In the pMSSM there is no information about how flavour violation in the soft-squared masses and trilinear terms generated by radiative corrections will impact flavour observables. We know that once full 3×3 Yukawa matrices are considered, flavour violation is automatically generated through radiative effects. In the MSSM-30, a counting rule keeps track of the hierarchical structure of the Yukawa matrices, expanded in terms of the Cabibbo angle, and the trilinear terms and soft squared masses are expanded in that basis. The off-diagonal parameters generated in that way can be thought as the effective off-diagonal parameters generated through radiative corrections. This rationale discards dangerous terms for FCNC and CP violation. In this sense, this work builds further on the project for MSSM explorations within systematically built frames with minimal theoretical or traditional prejudices and a Bayesian approach for deriving inference from experimental data [33, 8, 34, 35, 36, 37, 38, 39, 21, 40].

We emphasize that our approach is still model dependent, because of the way flavor is set at in [20] (there $Y_u = \lambda_u V$ and Y_d is diagonal where λ_u is the diagonal matrix of Yukawa couplings and V is the CKM matrix). With this realisation of MFV, the posterior sample from the MSSM-30 fit in [21] indicates results which supersedes those from the LHC search for gluinos and squarks. The MFV parametrisation naturally wants heavy gluinos and squarks. That was also the reason why a fit with logarithmic prior in the parameters was not done.

This work is organised as follows. In Sec. 2, we present a brief review of the MSSM-30 construction and the global fit of its parameters to data from indirect searches for BSM physics. The effect of the $B_s \rightarrow \mu^+ \mu^-$ measurement, and possible future accuracy in the measurement, on the MSSM-30 parameters is analysed there. In Sec. 3, we present respectively the numerical anatomy and analyses of the Wilson Coefficients, diagram-by-diagram, and particle-by-particle contributions to the $B_s \rightarrow \mu^+ \mu^-$ within the MSSM-30 frame. For some interesting points, we give comparisons and contrast the MSSM-30 results to the pMSSM case. The summary and conclusions are presented in Sec. 4.

2 The MSSM-30 parameters in light of the $B_s \rightarrow \mu^+ \mu^-$ observation

Here we briefly set the context of our analyses. First, the 30-parameter-MSSM frame is presented and contrasted with the pMSSM giving emphasis to the constraints on the two parameters most sensitive to the $\text{BR}(B_s \rightarrow \mu^+ \mu^-)$ observable. Second, the possible impact of future experimental precision in the $\text{BR}(B_s \rightarrow \mu^+ \mu^-)$ measurement is addressed. Finally, we comment on the possible impact of a future $\text{BR}(B_s \rightarrow \mu^+ \mu^-)$ precision measurement on the MSSM $(m_A, \tan \beta)$ plane.

2.1 The MSSM-30 frame

In [21] the minimal flavour violation MSSM parameters selection scheme leads to an MSSM frame with 30 parameters:

$$\underline{\theta} \equiv \{ M_{1,2,3}, \mu, M_A, \tan \beta, \text{Im}(M_{1,2}, \mu), \tilde{a}_{1,2,\dots,8}, \text{Im}(\tilde{a}_{4,5,8}), x_{1,2}, y_{1,3,4,5,6,7}, \text{Im}(y_{4,5}) \}, \quad (1)$$

which stem from the supersymmetry breaking terms,

$$\begin{aligned} & e^{\phi_1} M_1, \quad e^{\phi_2} M_2, \quad M_3, \quad \mu, \quad M_A, \quad \tan \beta, \quad e^{\phi_\mu}, \\ & M_Q^2 = \tilde{a}_1 + x_1 X_{13} + y_1 X_1, \quad X_1 = \delta_{3i} \delta_{3j}, \quad X_{13} = V_{3i}^* V_{3j} \\ & M_U^2 = \tilde{a}_2 + x_2 X_1, \\ & M_D^2 = \tilde{a}_3 + y_3 X_1, \\ & M_L^2 = \tilde{a}_6 + y_6 X_1, \\ & M_E^2 = \tilde{a}_7 + y_7 X_1, \\ & A_E = \tilde{a}_8 X_1, \\ & A_U = \tilde{a}_4 X_5 + y_4 X_1, \quad X_5 = \delta_{3i} V_{3j} \\ & A_D = \tilde{a}_5 X_1 + y_5 X_5. \end{aligned} \quad (2)$$

Here i and j run over as sparticles family indices, V is the SM CKM matrix and δ the Kronecker delta function. The gaugino mass parameters M_1, M_2 were allowed in the range -4 to 4 TeV for both real and imaginary parts. The gluino mass term is allowed in 100 GeV to 4 TeV. $\tilde{a}_{1,2,3,6,7} > 0$ were varied within the range $(100 \text{ GeV})^2$ to $(4 \text{ TeV})^2$ and $-(4 \text{ TeV})^2$ to $(4 \text{ TeV})^2$ for $x_{1,2}, y_{1,3,6,7}$. The trilinear coupling terms $\tilde{a}_{4,5,8}, \text{Im}(\tilde{a}_{4,5,8}), y_{4,5}$, and $\text{Im}(y_{4,5})$ are varied within -8 TeV to 8 TeV. m_A was allowed in 100 GeV to 4 TeV while the Higgs doublets mixing term $\mu, \text{Im}(\mu)$ in the range -4 to 4 TeV. In comparison, the pMSSM parameters are

$$\underline{\theta} = \{ M_{1,2,3}; m_{\tilde{f}_{Q,U,D,L,E}}^{3rd \text{ gen}}, m_{\tilde{f}_{Q,U,D,L,E}}^{1st/2nd \text{ gen}}; A_{t,b,\tau,\mu=e}, m_{H_{u,d}}^2, \tan \beta \}, \quad (3)$$

where $M_{1,2,3}$ are as for MSSM-30, $m_{\tilde{f}}$ the sfermion mass parameters were allowed in the range 100 GeV to 4 TeV. The trilinear couplings $A_{t,b,\tau,\mu=e} \in [-8, 8] \text{ TeV}$. The Higgs doublet masses $m_{H_1}^2, m_{H_2}^2$ were allowed according to $m^2 \in \text{sign}(m) [-4, 4]^2 \text{ TeV}^2$. $\text{sign}(\mu)$ is the sign

of the Higgs doublets mixing parameter (allowed to be randomly ± 1). The SM parameters were fixed at their experimentally determined central values for the MSSM-30 but varied in a Gaussian manner for the pMSSM.

The global fit of the MSSM-30 to Higgs boson mass, electroweak precision, B-physics, electric dipole moments and cold dark matter relic density measurements or limits were presented in [21]. The 2D posterior probability distribution on the $(m_A, \tan \beta)$ plane and a 3D scatter plot showing the variations of $\text{BR}(B_s \rightarrow \mu^+ \mu^-)$ are shown in Fig. 1 with updated $\text{BR}(B_s \rightarrow \mu^+ \mu^-)$ constrain [18]. The plot on Fig. 1 (top, left) shows the characteristic feature of the flat-prior MSSM-30 posterior with moderate to low $\tan \beta$ values and the relatively much less pronounced tendency towards sub-TeV values of m_A since the 95% Bayesian probability region, enclosed by the outer contour, basically spans over all the allowed range for m_A . The scatter plot in Fig. 1 (top, right) reveals an interesting observation: above some couple/few 100s of GeV, the $\text{BR}(B_s \rightarrow \mu^+ \mu^-) \sim 3.4 \times 10^{-9}$ is independent of m_A . In fact, restricting the $\text{BR}(B_s \rightarrow \mu^+ \mu^-)$ to within 15% combined measurement error around the value in [18] leads to the plot in Fig. 1 (bottom, left) showing that only light, sub-TeV values of m_A of the MSSM-30 sample could survive such precision. The link to the Wilson coefficients or particular sparticle contribution responsible for this feature will be addressed in Sec. 3.

For robust conclusions about the MSSM based on future $\text{BR}(B_s \rightarrow \mu^+ \mu^-)$ measurements with improved precision, the following points are important. First, the phenomenological frame for the MSSM predictions should be systematically constructed with minimised theoretical prejudices.

In this way, the MSSM-30 will be preferred compared to the pMSSM or the CMSSM. An explicit example of this can be seen in Fig. 1 (bottom, right) where we show the difference among the branching ratio $\text{BR}(B_s \rightarrow \mu^+ \mu^-)$ computed with a SLHA1-based input and micrOMEGAs, and with a SLHA2-based input computed with SPheno and SUSY_FLAVOR. For this comparison we used our MSSM-30 sample. Obviously the SLHA-2 is the correct interface for computing MSSM flavour observables. As such, the analyses presented in this article are based on the SUSY_FLAVOR package [45].

2.2 $\text{BR}(B_s \rightarrow \mu^+ \mu^-)$ prediction and measurement

The tagged average branching fraction of the rare decay $\text{BR}(B_s \rightarrow \mu^+ \mu^-)$ is given by

$$\begin{aligned} \text{BR}(B_s \rightarrow \mu^+ \mu^-) &= \frac{G_F^2 \alpha^2}{64\pi^3} f_{B_s}^2 m_{B_s}^3 |V_{tb} V_{ts}^*|^2 \tau_{B_s} \sqrt{1 - \frac{4m_\mu^2}{m_{B_s}^2}} \times \\ &\left[\left(1 - \frac{4m_\mu^2}{m_{B_s}^2}\right) \frac{m_{B_s}^2}{m_b^2} |C_S - C'_S|^2 + \left| \frac{m_{B_s}}{m_b} (C_P - C'_P) + 2(C_{10} - C'_{10}) \frac{m_\mu}{m_{B_s}} \right|^2 \right], \quad (4) \end{aligned}$$

where we follow the notation of [46], and the Wilson operators and coefficients are $\mathcal{H} = -\sum_{X,Y} O_{XY}^V C_{XY}^V + O_{XY}^S C_{XY}^S$, the vector operators are $O_{XY}^V = (d_J \gamma_\mu P_X d_I)(\ell_B \gamma^\mu P_Y \lambda_A)$, and the scalar operators are $O_{XY}^S = (d_J P_X d_I)(\ell_B P_Y \lambda_A)$, for $X, Y = L, R$ and P_X the chirality

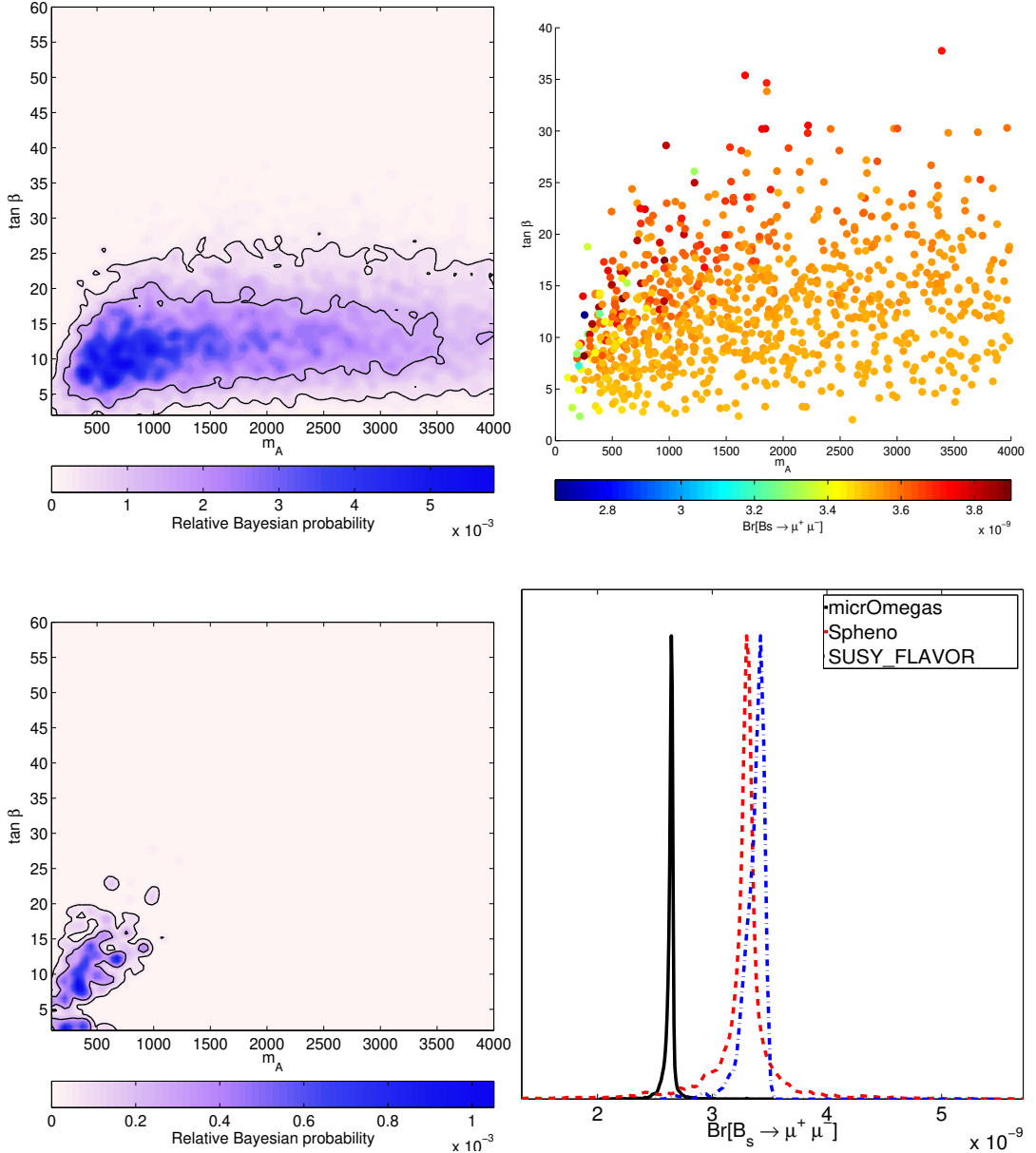


Figure 1: (Top left) The marginalised 2D MSSM-30 (m_A , $\tan\beta$) posterior distribution. The outer and inner contours enclose the 95% and 68% Bayesian probability regions respectively, m_A is in a GeV scale. (Top right) The scatter plot on the same plane shows the correlation to $\text{BR}(\text{B}_s \rightarrow \mu^+ \mu^-)$. (Bottom left) Plot for assessing the possible $\text{BR}(\text{B}_s \rightarrow \mu^+ \mu^-)$ precision impact on the (m_A , $\tan\beta$) plane. (Bottom right) Comparison of the branching ratio $\text{BR}(\text{B}_s \rightarrow \mu^+ \mu^-)$ as computed by different software and MSSM interfaces. With MICROMEGRAs [41] (solid/black line), the SLHA-1 [42] interface was used. SLHA-2 [43] inputs were used for computing the branching ratio with SPHENO [44] (dashed/red line) and SUSY_FLAVOR [45] (dashed-dot/blue line).

projectors. These operators are related to those of Eq. (4), as follows

$$\begin{aligned} C_S &= C_{LL}^S + C_{LR}^S, & C'_S &= C_{RR}^S + C_{RL}^S, \\ C_P &= -C_{LL}^S + C_{LR}^S, & C'_P &= C_{RR}^S - C_{RL}^S, \\ C_{10} &= -C_{LL}^V + C_{LR}^V, & C'_{10} &= C_{RR}^V - C_{RL}^V. \end{aligned} \quad (5)$$

We use SUSY_FLAVOR [45] to obtain the contributions from the different particles and kinds of diagrams ¹, Higgs and Z penguins and box diagrams. In this software, the contributions to Eq. (4) are expressed in terms of the coefficients F_S , F_P and F_A related to the Wilson coefficients of Eq. (5) as Eqs. (2.6-2.9) of [48], which are

$$\begin{aligned} F_S &= \frac{i}{4} \frac{m_{B_s}^2 f_{B_s}}{m_b + m_s} (C_S - C'_S), \\ F_P &= \frac{i}{4} \frac{m_{B_s}^2 f_{B_s}}{m_b + m_s} (C_P - C'_P), \\ F_A &= -\frac{i}{4} f_{B_s} (C_{10} - C'_{10}). \end{aligned} \quad (6)$$

It is well established that in the SM, C_{10} gets its larger contribution from the Z penguin with a top loop, about 75% and its second largest contribution from the W box, 24% and we have

$$\text{BR}(B_s \rightarrow \mu^+ \mu^-)^{\text{SM}} = (3.25 \pm 0.17) \times 10^{-9}. \quad (7)$$

The experimental measured quantity (denoted here with an overline) is the untagged branching fraction which is related to Eq. (4), the theoretical (tagged) expression, as

$$\overline{\text{BR}}(B_s \rightarrow \mu^+ \mu^-) = \left[\frac{1 - y_s^2}{1 + \mathcal{A}_{\Delta\Gamma}^{\mu\mu} y_s} \right] \overline{\text{BR}}(B_s \rightarrow \mu^+ \mu^-), \quad (8)$$

where $ys = \Delta\Gamma_s / 2\Gamma_s$, $\Delta\Gamma_s$ being the decay width difference between the B_s mass eigenstates and $\Gamma_s = \tau_{B_s}^{-1}$ is the average B_s decay width, using the LHCb measurement ($y_s = 0.087 \pm 0.014$ [49]), and that in the SM $\mathcal{A}_{\Delta\Gamma}^{\mu\mu} = 1$, we obtain

$$\overline{\text{BR}}(B_s \rightarrow \mu^+ \mu^-)^{\text{SM}} = (3.56 \pm 0.18) \times 10^{-9}, \quad (9)$$

on the other hand, the experimental value measured by the LHCb collaboration is [18, 19], including Run 1 and Run 2 data,

$$\overline{\text{BR}}(B_s \rightarrow \mu^+ \mu^-) = (3.0 \pm 0.6^{+0.3}_{-0.2}) \times 10^{-9}. \quad (10)$$

while the CMS value is [50],

$$\overline{\text{BR}}(B_s \rightarrow \mu^+ \mu^-) = (2.8 \pm 0.5^{+0.3}_{-0.2}) \times 10^{-9}. \quad (11)$$

¹ For this case, we use a modified version of the program, for which we have explicitly checked those contributions with the help of references [6, 46, 47, 1, 2, 48].

As we can see, both values in agreement with the SM. In the MSSM, $\mathcal{A}_{\Delta\Gamma}^{\mu\mu} = (|P|^2 \cos(2\varphi_P) - |S|^2 \cos(2\varphi_S)) / (|P|^2 + |S|^2)$, [51], where $\varphi_S = \arg(S)$, $\varphi_P = \arg(P)$, and S and P are related to our notation for the Wilson Coefficients as follows

$$S = \sqrt{1 - 4 \frac{m_\mu^2}{m_{B_s}^2} \frac{m_{B_s}^2}{2m_\mu} \frac{1}{m_b + m_s} \frac{C_S - C'_S}{C_{10}^{SM}} \frac{m_{B_s}}{m_b}}, \quad (12)$$

$$P = \frac{C_{10}}{C_{10}^{SM}} + \frac{m_{B_s}^2}{2m_\mu} \frac{1}{m_b + m_s} \frac{C_P - C'_P}{C_{10}^{SM}} \frac{m_{B_s}}{m_b}. \quad (13)$$

In the upper panels of Fig. 2 we compare the planes $\tan\beta$ vs the tagged value of $\text{BR}(B_s \rightarrow \mu^+\mu^-)$ (top-left), as produced by the official 2.53 version of *SUSY_FLAVOR*, and $\tan\beta$ vs the untagged value of $\text{BR}(B_s \rightarrow \mu^+\mu^-)$ (top-right) using a modified version of it. This comparison shows the importance of appropriately comparing the measurement of the $\text{BR}(B_s \rightarrow \mu^+\mu^-)$ with the theoretical value. Although the contributions from the pre-factors in Eq. (8) do not differ greatly from point to point (due to the smallness of the supersymmetric contributions), they have a significant impact in pushing up the values of $\text{BR}(B_s \rightarrow \mu^+\mu^-)$. In the lower part of the figure we present just the tagged distribution for the linear prior of the pMSSM, which is in agreement with that of [9]. In the plane $\tan\beta$ vs $\text{BR}(B_s \rightarrow \mu^+\mu^-)$ is clear that for the MSSM-30, contrary to the pMSSM, values of $\tan\beta < 10$ are not excluded. This shows that allowing a richer structure in the soft-squared terms, opens up regions of parameter space in comparison to the pMSSM. One of the main results of this work is that for the MSSM-30 is possible to find larger values of $\text{BR}(B_s \rightarrow \mu^+\mu^-)$ for $\tan\beta \in (10, 20)$, which is not possible in the pMSSM.

From the second plot of Fig. 2, we can see that supersymmetric contributions add up little to the SM contribution, except for values between $\tan\beta \sim (10, 20)$, where there could be both enhancing or suppressing effects. In Sec. 3, we present the numerical anatomy of the $\text{BR}(B_s \rightarrow \mu^+\mu^-)$ based on the MSSM-30 frame for which there are sources for CP violation beyond the CKM. We shall comment just on the interplay of the contributions coming from the neutral Higgs, H^0 and Z penguin diagrams after introducing the theory of supersymmetric contributions to C_S , C_P and C_{10} . We do not comment on the the box diagram contribution to any of the Wilson coefficients entering into $\text{BR}(B_s \rightarrow \mu^+\mu^-)$ because it remains small in comparison to the SM [46], in the region of low $\tan\beta$. Although this is strictly true in the case where the CKM matrix is the only source of CP and flavour violation, in our case the contributions from the extra sources of CP violation are negligible.

3 MSSM-30 contributions to $B_s \rightarrow \mu^+\mu^-$

For the MSSM-30 there are new sources of flavor and CP violation beyond the CKM and therefore the contribution from different particles becomes relevant. As it will be shown later, the neutralino and gluino contributions can compete with those from charginos. Although all of these contributions are suppressed in the MSSM-30 posterior sample with $\tan\beta$ typically less than 30. Therefore, for making contrast to the various BSM contributions within the pMSSM and MSSM-30, different regimes for $\tan\beta$ are considered.

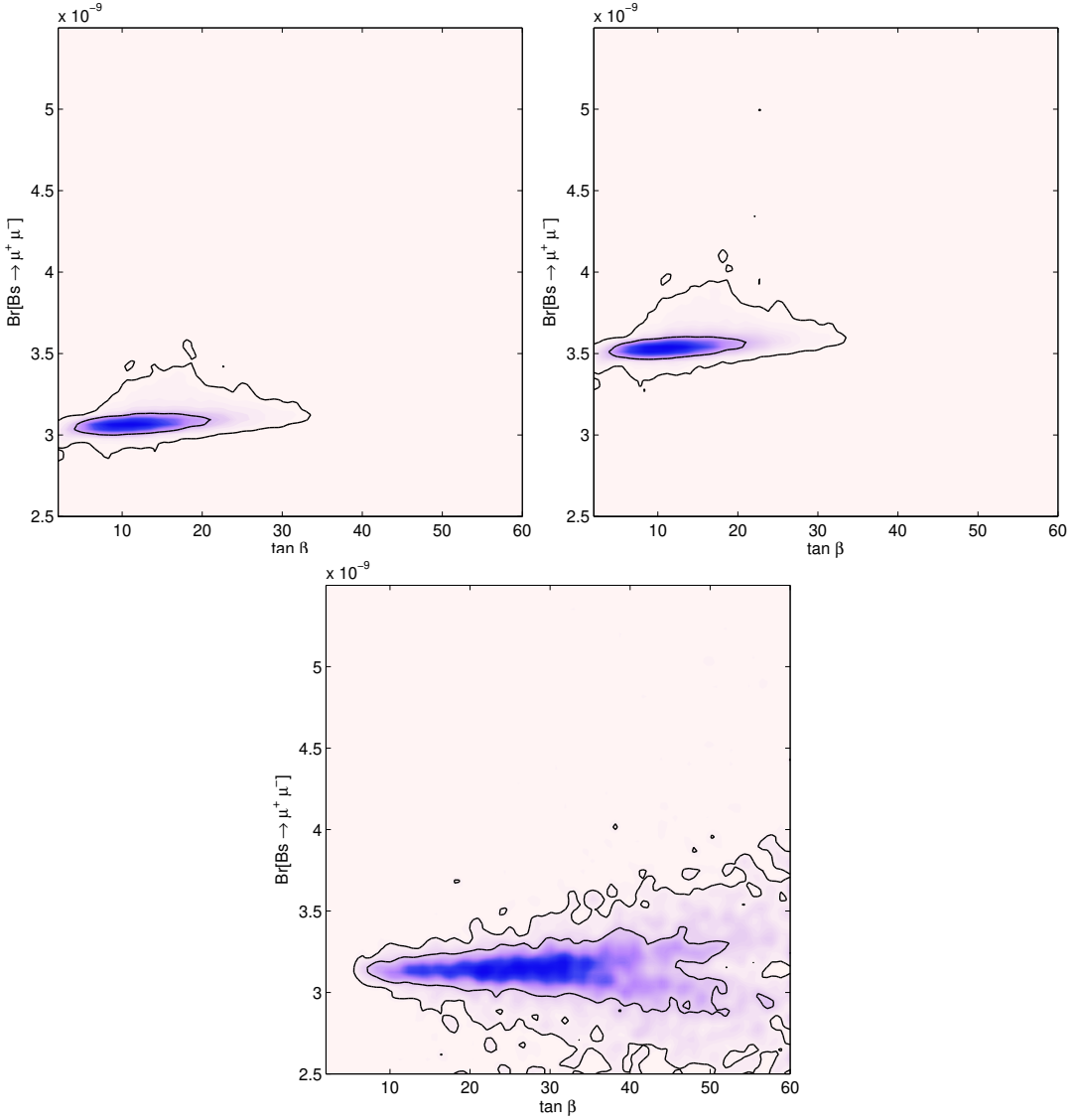


Figure 2: $\tan \beta$ vs $\text{BR}(B_s \rightarrow \mu^+ \mu^-)$ for the MSSM-30 sample (top) and for the pMSSM (bottom). For the MSSM-30 sample we have plotted (left) the tagged contribution as produced by the official 2.53 version of *SUSY_FLAVOR* and the untagged values (right) using a modified version of it. One of the main results of our work is to note that whereas values for $\tan \beta < 10$ are excluded in the pMSSM, for the MSSM-30 such low values of $\tan \beta$ are possible.

3.1 Diagram-by-diagram and particle-by-particle contributions

From here on, we refer to the Box, Higgs penguin and Z penguin diagrams, for which some examples are shown in Fig. 5. As mentioned before, C_{10} gets its larger contribution from the Z penguin with a top loop, about 75% and its second largest contribution from the W box, 24%. Higgs penguin contributions from SM are highly suppressed. On the other hand, the largest contribution in the pMSSM comes from the second diagram of Fig. 5 since the degeneracy of scalar masses \tilde{Q} is broken by radiative effects induced by Yukawa couplings. This produces an effective flavor off-diagonal piece which does not go away when rotating to mass eigenstates basis [6]. In the MSSM-30 off-diagonal elements are present and compete with the contribution coming from the aforementioned radiative effects. Contributions from the Z penguin diagrams are in general suppressed, except for low value of $\tan\beta$ ($\lesssim 10$).

In Fig. 3 and Fig. 4 we compare the pMSSM and the MSSM-30 in terms of their contributions to $\text{BR}(B_s \rightarrow \mu^+ \mu^-)$ coming from different diagrams and particles respectively. The contributions for the pMSSM (solid black lines) are compared to the MSSM-30 case (red dashed lines). We can see that the distributions for the Z penguin and Box diagrams become narrower in the MSSM-30, in comparison to those of the pMSSM, but overall these contributions shift $\text{BR}(B_s \rightarrow \mu^+ \mu^-)$ to higher values than in the pMSSM case. For the MSSM-30, the contributions to the Higgs-Penguin diagrams become a bit suppressed, because of the preferred bigger masses for m_A and $m_{\tilde{t}}$ and lower values for $\tan\beta$.

3.2 Contributions to C_P and C_S

H^0 -penguin

As mentioned above, the most important contribution in the pMSSM comes from the Higgs penguin diagram depicted in the second diagram of Fig. 5. This happens because the degeneracy of scalar masses \tilde{Q} is broken by radiative effects induced by Yukawa couplings and hence this induces an effective flavor off-diagonal piece which does not go away when rotating to mass eigenstate basis [6]. The large $\tan\beta$ region of this contribution can play a very significant role. This can be understood by writing the simplified contribution at LO as [1]

$$\begin{aligned} C_S^{H^0}(\tilde{\chi}^\pm) &\approx -C_P^{H^0}(\tilde{\chi}^\pm) \\ &= \mu A_t \frac{\tan^3 \beta}{(1 + \epsilon_b \tan \beta)^2} \frac{m_t^2}{m_{\tilde{t}}^2} \frac{m_b m_\mu}{4 M_W^2 m_A^2 \sin^2 \theta_W} x \left[\frac{(1-x) + \log(x)}{(1-x)^2} \right], \\ x &= m_{\tilde{t}}^2 / m_{\tilde{\chi}_1^\pm}^2, \quad m_{\tilde{\chi}_1^\pm} \approx \mu, \end{aligned} \quad (14)$$

which is quite sensitive to m_A and $m_{\tilde{t}}$ and therefore drops noticeably with the increase of their values. From this expression, we can also understand that the lower the value of $\tan\beta$, the lower the contribution to $\text{BR}(B_s \rightarrow \mu^+ \mu^-)$ from this diagram. Since for our fits, the preferred values of $m_{\tilde{t}}$ are $O(1)$ TeV for the pMSSM, the suppression of this contribution becomes considerable.

In the MSSM-30, the off-diagonal parameters in the soft-squared masses and trilinear terms, Eq. (1), add up to the contributions given by the broken degeneracy of the scalar

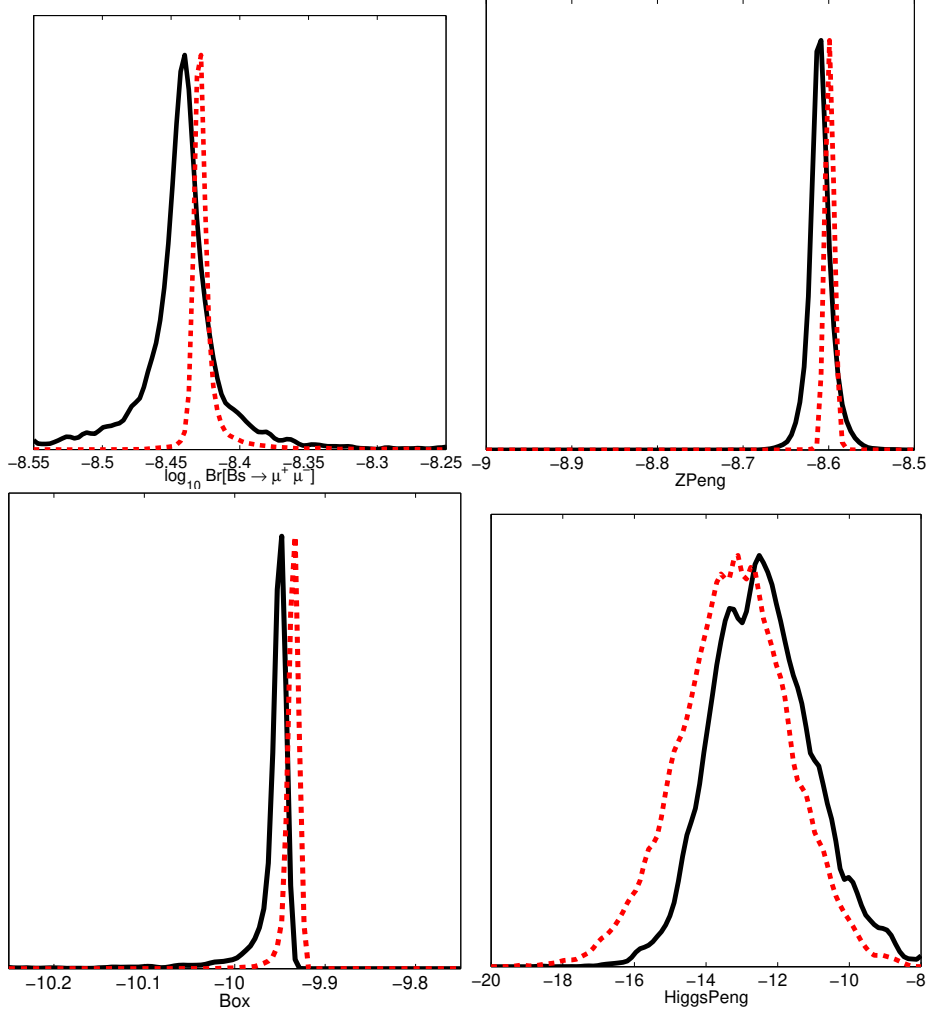


Figure 3: Contribution by diagrams to $\text{BR}(B_s \rightarrow \mu^+ \mu^-)$. The solid black lines correspond to the pMSSM and the dashed red lines to the MSSM-30. The distributions for the Z penguin and Box diagrams become narrower in the MSSM-30 in comparison to those of the pMSSM, but overall these contributions shift $\text{BR}(B_s \rightarrow \mu^+ \mu^-)$ to higher values than in the pMSSM case. For the MSSM-30, the contributions to the Higgs-Penguin diagrams become suppressed, due to the preferred bigger masses for m_A and $m_{\tilde{t}}$ and lower values for $\tan \beta$. For all plots, the vertical axis represent the relative probability density associated to a point in the MSSM scan. The horizontal axis is the logarithm of the corresponding contribution to $\text{BR}(B_s \rightarrow \mu^+ \mu^-)$.

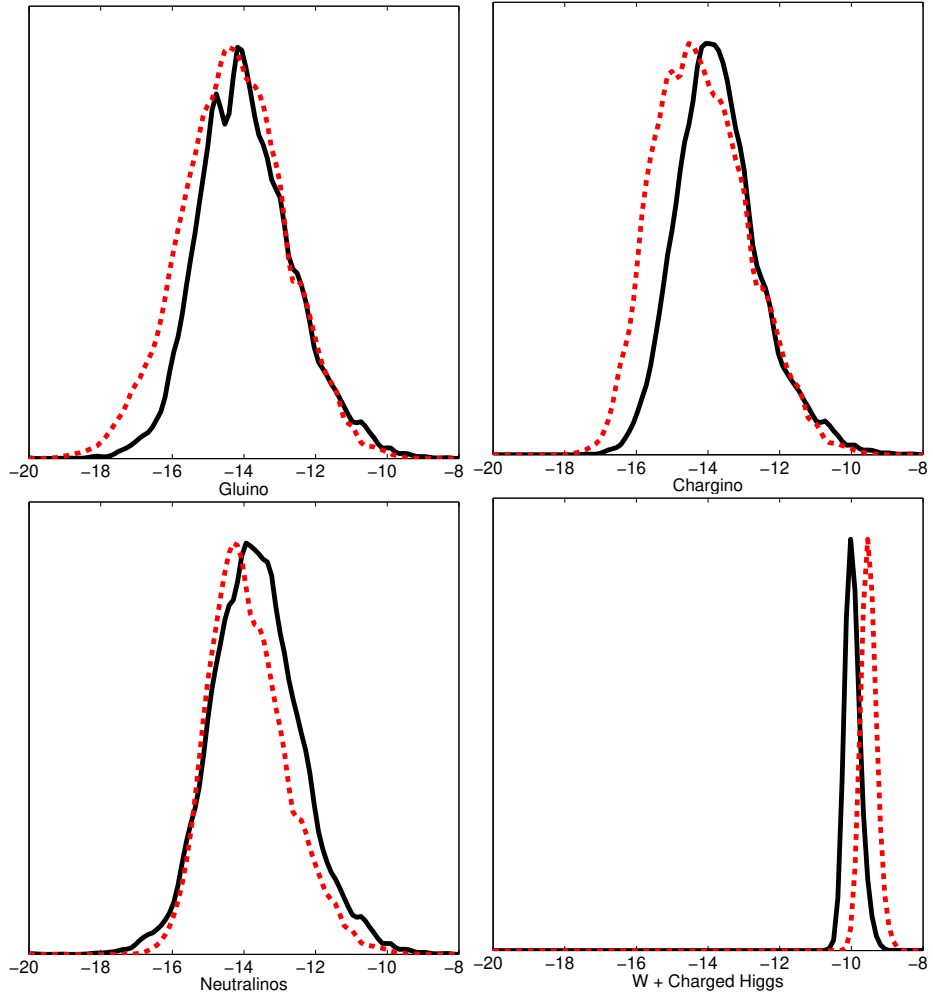


Figure 4: The particle-by-particle contributions to $\text{BR}(B_s \rightarrow \mu^+ \mu^-)$. The solid black lines correspond to the pMSSM and the dashed red lines to the MSSM-30. In SUSY_FLAVOR the charged-Higgs contribution cannot be separated from the SM W-boson contribution. The axes are as in Fig. 3.

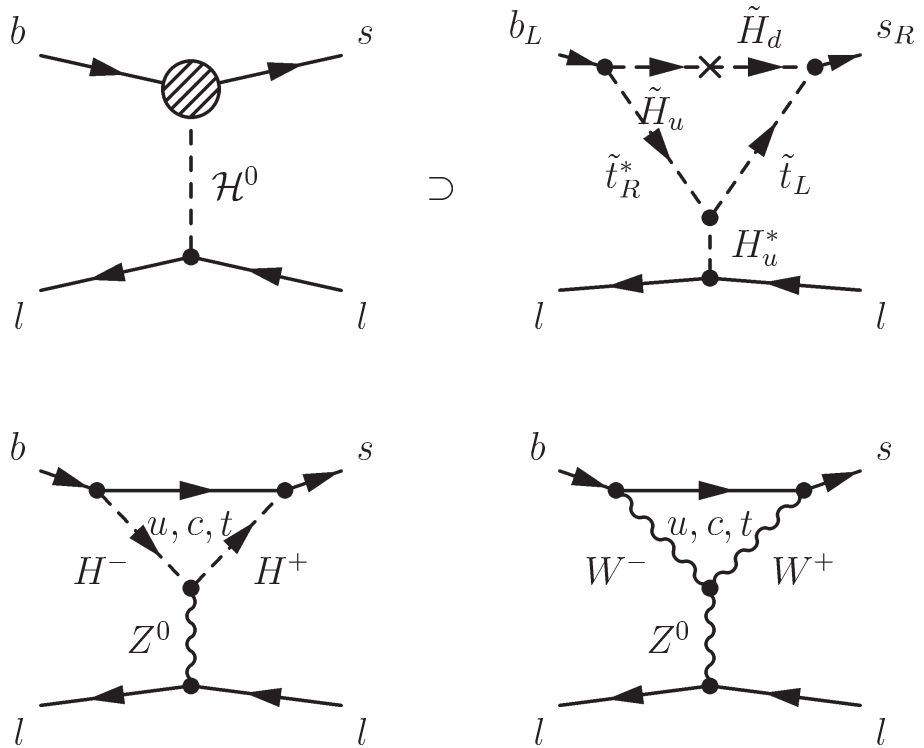


Figure 5: Higgs penguin and Z penguin diagrams contributing to $\text{BR}(B_s \rightarrow \mu^+ \mu^-)$. The first diagram represents the general Higgs penguin diagram. The most important contribution in the pMSSM comes from the second diagram of the first line, depicted in flavour basis. Even in the pMSSM this is the most important contribution since the degeneracy of scalar masses \tilde{Q} is broken by radiative effects induced by Yukawa couplings and hence induces an effective flavor off-diagonal piece which does not go away when rotating to mass eigenstates basis [6]. The last Z penguin gives the leading SM contribution.

masses \tilde{Q} . In this case, the contributions to $C_{S,P}^{H^0}(\tilde{\chi}^\pm)$ cannot be written in the form of Eq. (14), because non-zero off-diagonal terms are present even before the breaking of the degeneracy of the diagonal soft-squared masses. However, we find that the differences between the contributions of $C_{S,P}^{H^0}(\tilde{\chi}^\pm)$ in the pMSSM and in the MSSM-30 is only at the percent level. In this respect, in the MSSM-30, there could cancellations between these with other equally heavy/high magnitude parameters (e.g. μ and A_t). These cancellations could make the $\text{BR}(B_s \rightarrow \mu^+\mu^-)$ independent of m_A as shown in Fig. 2 (top-right), and make the contribution to the Wilson Coefficients not so different from the pMSSM.

Z-penguin

Supersymmetric particles propagating in the loop cannot generate a contribution to $C_{S,P}, C'_{S,P}$ due to the vector coupling to Z^0 .

3.3 Contributions to C_{10}

H^0 -penguin

For the large $\tan \beta \geq 30$ regime, the neutral Higgs boson couplings to the down-type quarks and charged leptons are enhanced by $\tan \beta$ factors and so the contribution from the charged Higgs in the loop becomes important.

Z-penguin

For charged Higgs and low values of $\tan \beta \leq 20$, Higgs penguin and box diagrams are small. Hence, the contribution from the Z (third diagram in Fig. 5) penguin becomes the dominant one among all of the contributions to C_{10} . This effect becomes accentuated for very small values of $\tan \beta$.

Our fits favor intermediate values of $\tan \beta$, so in principle there is a transition between the regimes of H^0 and Z penguin dominance. However, this also depends on the values of the charged-Higgs mass and most importantly on the value of m_H , being large, there is not a surprise that both contributions are mostly suppressed. At LO, the corresponding contributions to C_{10} and C'_{10} are [1]

$$\begin{aligned} C_{10}^Z(H^\pm) &= \frac{1}{8 \sin_W^2} \frac{m_t^2}{m_W^2} \frac{1}{\tan^2 \beta} f_H(y_t), \\ C'_{10}^Z(H^\pm) &= -\frac{1}{8 \sin_W^2} \frac{m_s m_b}{m_W^2} \tan^2 \beta f_H(y_t), \\ f_H(y_t) &= \frac{y_t}{1 - y_t} \left(1 + \frac{1}{1 - y_t} \log y_t \right), \quad y_t = m_t^2 / m_{H^\pm}^2. \end{aligned} \quad (15)$$

Using SUSY_FLAVOR we find that the total contribution to C_{10} is $C_{10T}^Z(H^\pm) = C_{10}^Z(H^\pm) - C'_{10}^Z(H^\pm) \in (O(10^{-3}), O(10^{-2}))$, adding up little to the total of C_{10} , including the SM contributions. For our set of experimental values we obtain $C_{10}^{\text{SM}} = -4.40 \pm 0.05$. In the SM the current accuracy for this coefficient is better than 0.1% level when allowing only the

top-quark mass and the strong coupling constant to deviate from their corresponding central value [52].

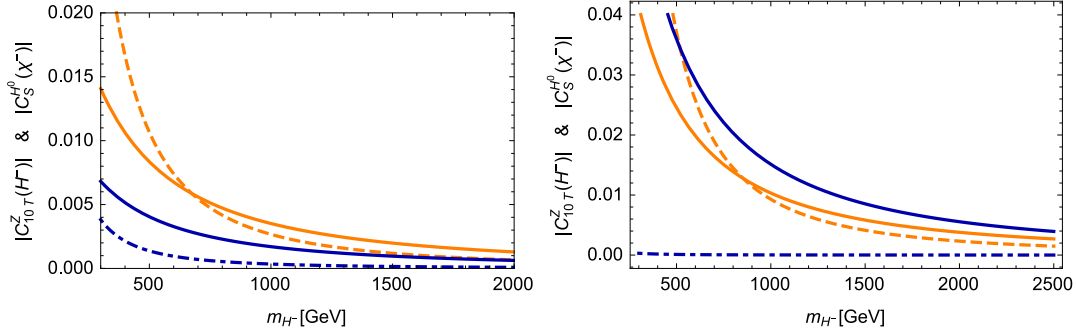


Figure 6: $|C_{10T}^Z(H^\pm)|$ and $|C_S^{H^0}(\chi^\pm)|$ as a function of $m_{H^\pm} (\approx m_A)$. The solid lines correspond to $|C_{10T}^Z(H^\pm)|$ and the dashed and dot-dashed to $|C_S^{H^0}(\chi^\pm)|$. In both plots, the orange (light) lines correspond to the higher value of $\tan \beta$, while the dark (blue) to the lower value of $\tan \beta$. For both plots, $(A_t, m_{\tilde{t}}, \mu) = (1200, 1200, 100)$ GeV. For the left panel, the two values of $\tan \beta$ are 25 (high) and 12 lower. These values correspond respectively to the typical values for the pMSSM and the MSSM-30 sample. For the right panel, we plotted the extreme values of the MSSM-30 sample, $\tan \beta = 5, 40$, where we can appreciate the enhancement of $|C_{10T}^Z(H^\pm)|$ for small values of $\tan \beta$.

For illustration of our discussion, in Fig. 6 we have made a comparison at LO of $C_{10T}^Z(H^\pm)$ and $C_S^{H^0}(\chi^\pm)$ to emphasise the importance of the values of m_{H^-} and $\tan \beta$ in order to determine from which kind of diagram the contributions to $\text{BR}(B_s \rightarrow \mu^+ \mu^-)$ are the most important.

Although in general for heavy spectra, both contributions are really small in comparison to the SM contributions, one can still appreciate the relevance of some supersymmetric particles. The solid lines correspond to $C_{10T}^Z(H^\pm)$ and the dashed and dot-dashed to $C_S^{H^0}(\chi^\pm)$. For both plots, $(A_t, m_{\tilde{t}}, \mu) = (1200, 1200, 100)$ GeV. For the left panel the two values of $\tan \beta$ are 25 (high) and 12 lower. These values correspond respectively to the typical values for the pMSSM and the MSSM-30 sample. For the right panel, we plotted the extreme values of the MSSM-30 sample, $\tan \beta = 5, 40$.

We can see that, as it is well established, for values of m_{H^-} below 1 TeV, the contribution from the large $\tan \beta$ values (here 25) coming from $C_S^{H^0}(\chi^\pm)$ is the leading one (in Fig. 6 represented by the orange-light-dashed line). On the other hand, contributions to both $C_{10T}^Z(H^\pm)$ and $C_S^{H^0}(\chi^\pm)$ for values of $\tan \beta$ around 10 are typically less than a third of the corresponding values when $\tan \beta > 20$. Since for the pMSSM sample, values for $\tan \beta$ above 20 dominate the sample, it is clear that the most important contributions come from $C_S^{H^0}(\chi^\pm)$. For the MSSM-30 sample however, smaller values than 10 for $\tan \beta$ are an important part of the sample and in this case they can give the largest supersymmetric contribution to the Wilson-Coefficients via $C_{10T}^Z(H^\pm)$. This is appreciated in the plot of the left in Fig. 6 where $C_{10T}^Z(H^\pm)$ for $\tan \beta = 5$ and $m_{H^-} > 700$ GeV is the dominant of the supersymmetric contributions (solid blue-dark line).

One of the main results of this work is that for the MSSM-30 is possible to find larger values of $\text{BR}(B_s \rightarrow \mu^+ \mu^-)$ for $\tan \beta \in (10, 20)$, which is not possible in the pMSSM.

3.4 Interplay of Wilson coefficients

In order to understand the different contributions to Eq. (4), it is customary to compare the relative size of the Wilson Coefficients C_S and C_P to C_{10} . This is useful because C_S and C_P can only have supersymmetric contributions and supersymmetric contributions to C_{10} are highly suppressed.

In order to do this comparison, we compare the value of C_{10} to the Wilson Coefficients C_S and C_P but weighted in the same way that C_{10} contributes to $\text{BR}(B_s \rightarrow \mu^+ \mu^-)$, Eq. (4). This allows a direct comparison among C_S , C_P and C_{10} . The weighted Wilson Coefficients C_S and C_P are respectively denoted by \hat{C}_S and \hat{C}_P :

$$\begin{aligned}\hat{C}_S &\equiv \frac{m_{B_s}^2}{2m_\mu m_b} \sqrt{1 - \frac{4m_\mu^2}{m_{B_s}^2}} C_S \\ \hat{C}_P &\equiv \frac{m_{B_s}^2}{2m_\mu m_b} C_P.\end{aligned}\quad (16)$$

In Fig. 7, we plot our results in planes C_{10} vs \hat{C}_S (we do not present C_{10} vs \hat{C}_P since $\hat{C}_S \approx -\hat{C}_P$), comparing the Wilson Coefficients for the two samples. For the pMSSM sample we present only the results when fixing the top mass value, since for our MSSM-30 sample the top mass was kept fixed. In this sense, even if the sample is not complete for the pMSSM, we give a fair comparison to the MSSM-30 sample and we can be sure that the increase (in absolute value) of the Wilson Coefficient C_{10} arises due to the supersymmetric contributions. Within the pMSSM frame $C_{10} = -4.58 \pm 0.06$ ranging from -4.68 to -4.50 at 95% Bayesian probability region. For the MSSM-30, $C_{10} = -4.64 \pm 0.01$ ranging from -4.66 to -4.63 at 95% Bayesian probability region. Overall the contour plots for C_{10} vs C_S and C_{10} vs C_P cover a bigger area in the pMSSM (see also e.g. [9]) than in the MSSM-30 but the one and two sigma regions of this last sample are shifted to the left, Fig. 7. As mentioned in Section 3.2, at the LO, we obtain $C_{10}^{SM} = -4.40 \pm 0.05$ and the current accuracy is of the order 0.1%. The MSSM contributions can contribute to C_{10} at the $O(10^{-1})$ and therefore could be disentangled from the SM uncertainty.

From Fig. 6 we can see that for large values of m_{H^-} (> 1500 GeV) the contributions from $|C_{10T}^Z(H^\pm)|$ and $|C_S^{H^0}(\chi^\pm)|$ become quite similar, specially for lower values of $\tan\beta$ (approximately below 20). On the other hand, since for the pMSSM sample, values for $\tan\beta$ above 20 dominate the sample, the most important contributions come from $C_S^{H^0}(\chi^\pm)$. For the MSSM-30 sample however, smaller values than 10 for $\tan\beta$ are an important part of the sample and in this case they can give the largest supersymmetric contribution to the Wilson-Coefficients via $C_{10T}^Z(H^\pm)$, as mentioned before (Fig. 6).

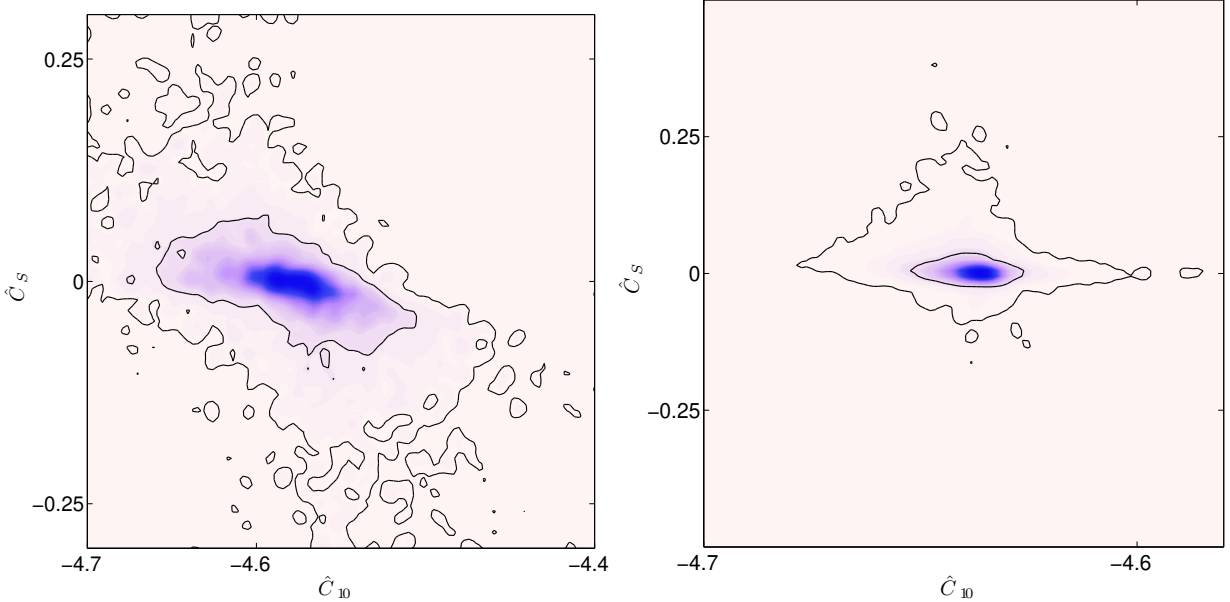


Figure 7: We compare here the Wilson Coefficients C_{10} , C_S and C_P for the pMSSM sample (left) and for the MSSM-30 sample (right). Within the pMSSM frame $C_{10} = -4.58 \pm 0.06$ ranging from -4.68 to -4.50 at 95% Bayesian probability region. For the MSSM-30, $C_{10} = -4.64 \pm 0.01$ ranging from -4.66 to -4.63 at 95% Bayesian probability region.

3.5 Interplay of off-diagonal soft-squared elements

It is customary to assess the impact of flavor violation in terms of the flavor violating parameters

$$\delta_{QXY}^{ij} = \frac{(M_Q^2)^{ij}_{XY}}{\sqrt{(M_Q^2)^{ii}_{XX} (M_Q^2)^{jj}_{YY}}}, \quad (17)$$

which measure the amount of off-diagonal allowed contributions, in our case constrained by the $\text{BR}(B_s \rightarrow \mu^+ \mu^-)$ observable. In order to make manifest how the Z penguin contributions dominate the supersymmetric contributions of the coefficient C_{10} for most part of the parameter space. We present in Fig. 8 (top row) the individual contributions to $\text{BR}(B_s \rightarrow \mu^+ \mu^-)$ from Higgs penguin, Z penguin and Box diagrams, as a function of $(\delta_{QLR})^{23}$.

We can there clearly appreciate how Z penguin contributions are in general the most dominant for practically all values of $(\delta_{QLR})^{23}$ and as emphasized in [46], for small values of $\tan \beta$ (≤ 20), Higgs penguin contributions are small. Box contributions are also small, and they tend to be even bigger than the Higgs penguin contributions. In the second row of Fig. 8 we represent the individual contributions to $\text{BR}(B_s \rightarrow \mu^+ \mu^-)$ from Higgs penguin, Z penguin and Box diagrams, as a function of $(\delta_{QLL})^{23}$. As it is usual with LR flavour violation, it tends to be more constrained, as in this case it is allowed to be only $O(10^{-3})$, while LL flavour violation it can be of $O(10^{-2})$.

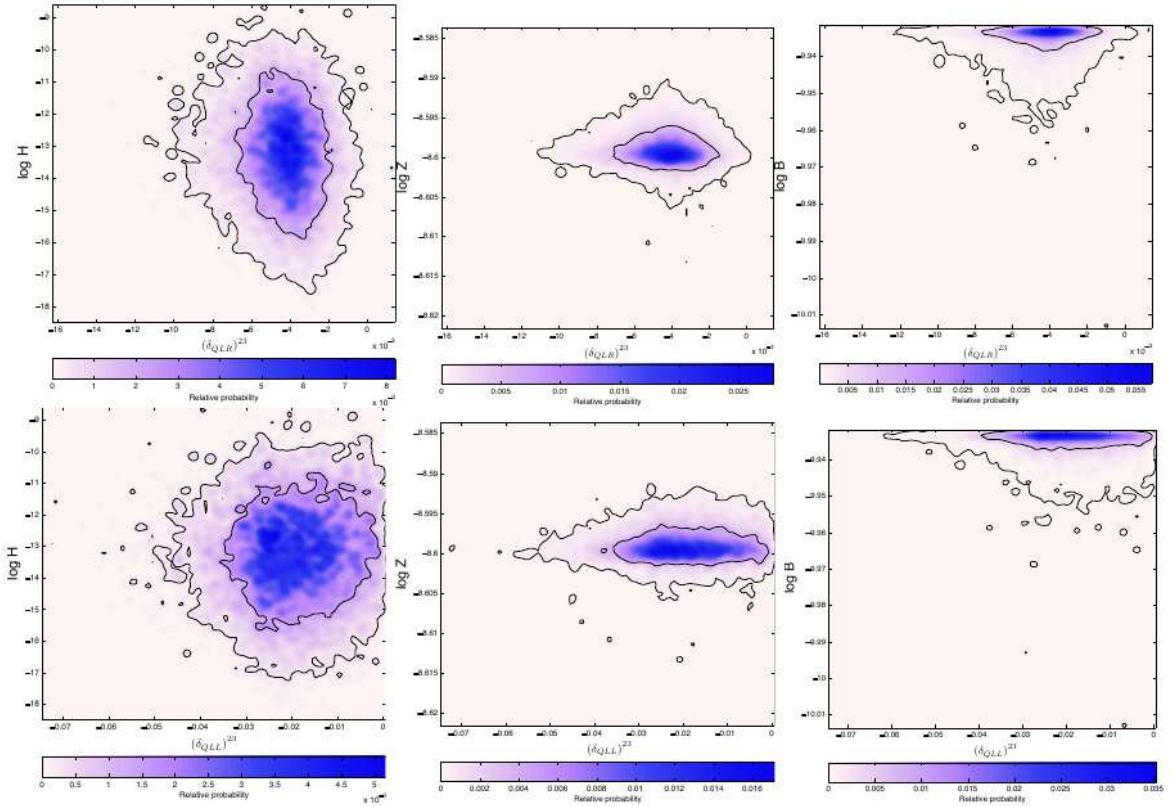


Figure 8: Contributions to $\text{BR}(B_s \rightarrow \mu^+ \mu^-)$ from the parameters $(\delta_{QLR})^{23}$ and $(\delta_{QLL})^{23}$ (top and bottom rows respectively). $\log H$, $\log Z$ and $\log B$ represent respectively the logarithms of the Higgs Penguin, Z penguin and Box contributions to the total $\text{BR}(B_s \rightarrow \mu^+ \mu^-)$.

4 Conclusions

We have continued with our studies in order to explore features of the MSSM by using Bayesian statistical techniques on systematically constructed, symmetry-guided, MSSM frames beyond the traditional constructions. Here, the phenomenological frame considered is the 30-parameter-MSSM, called MSSM-30, and the observable of interest is the $B_s \rightarrow \mu^+ \mu^-$ decay. The measured branching ratio $\text{BR}(B_s \rightarrow \mu^+ \mu^-)$ is compatible with the SM prediction but it still has a large (order 20%) uncertainty. Future precision measurements of this observable will be excellent for assessing the MSSM as New Physics beyond the SM. Within the MSSM-30 a posterior sample was considered, for which a 15% uncertainty on the measured $\text{BR}(B_s \rightarrow \mu^+ \mu^-)$ would favour a sub-TeV pseudo-scalar Higgs boson. The outcome would have been completely different had the pMSSM limit of the MSSM-30 sample been used for computing the $\text{BR}(B_s \rightarrow \mu^+ \mu^-)$ as shown in Fig. 1.

Knowing that the decay $B_s \rightarrow \mu^+ \mu^-$ is a good indicator for assessing models with extended Higgs sectors, we compare the MSSM-30 along the pMSSM frames to see if there is any physics or features in the parameters of the former which are not accessible in the later. It turned out to be the case since the MSSM-30 sample prefers lower values of $\tan \beta \sim (10, 20)$, in comparison to the pMSSM which prefers $\tan \beta \sim (20, 40)$. This makes possible to find higher values for $\text{BR}(B_s \rightarrow \mu^+ \mu^-)$ in the MSSM-30 mainly due to bigger contributions coming from diagrams involving charginos and Z-penguin diagrams. This is one of the main results of this work.

We found that the best way to analyse the contributions to the branching ratio $\text{BR}(B_s \rightarrow \mu^+ \mu^-)$ was by comparing between diagrams: Z penguin, Box and Higgs Penguin diagrams instead of by contributions among supersymmetric particles (i.e. gluinos, neutralinos or charginos). The reason is that in the pMSSM the supersymmetric contributions become quite suppressed due to the large values of m_A and $m_{\tilde{t}}$ (well into multi-TeV region) and that in the SM the Z penguin and box contributions are dominant ($\sim 75\%$ and 24% respectively). This last fact then in principle helps to spot for contributions coming from supersymmetry. In the pMSSM it is well established that the contributions coming from a Higgs penguin and a chargino in the loop gives the most important contribution, so this is a specific example of how analysis by kind of diagrams becomes relevant.

The MSSM-30 has by construction non-zero off-diagonal soft-squared mass terms, contrary to the pMSSM where they are set to zero by hand. When analysing both samples using a Bayesian fit, both samples are constrained to the same observables. Therefore, if no cancellations appear, the value of the effective allowed off-diagonal soft-squared mass terms should be of the same order in both samples. The best place to look for the difference between both samples is in the contribution coming from the charginos, mainly from Higgs-Penguins, (Fig. 4), were we can see that the distributions from pMSSM and MSSM-30 are different but mostly indistinguishable towards higher values of the distribution.

In order to assess the impact of contributions to B observables, beyond the SM ones, it is customary to compare the size of the Wilson Coefficients which receive the majority of the BSM contributions with the Wilson Coefficients present only in the SM case. For the decay $B_s \rightarrow \mu^+ \mu^-$, the relevant coefficients are C_S and C_P , which are scalar operators sensitive to the chirality of BSM contributions. In the SM the only contribution comes from

the vector operator C_{10}^{SM} , for which we find a value of -4.13 ± 0.05 . We have compared the coefficients C_S and C_P to C_{10} , using C_{10} vs C_S and C_{10} vs C_P planes and found that in the MSSM-30, C_S and C_P represent typically only a $O(1\%)$ contribution to the branching ratio $B_s \rightarrow \mu^+ \mu^-$. Within the pMSSM frame $C_{10} = -4.58 \pm 0.06$ ranging from -4.68 to -4.50 at 95% Bayesian probability region. For the MSSM-30, $C_{10} = -4.64 \pm 0.01$ ranging from -4.66 to -4.63 at 95% Bayesian probability region. The MSSM-30 is more severely away from the SM value compared to the pMSSM. The current SM accuracy in determining the value of C_{10} is of the order 0.1% and therefore supersymmetric contributions can be disentangled from the SM uncertainty.

Finally, as an outlook we highlight that future improvements on the measurement of $\text{BR}(B_s \rightarrow \mu^+ \mu^-)$, along with the measurement of other observables, like $\mathcal{A}_{\Delta\Gamma}^{\mu\mu}$ and $\text{BR}(B_d \rightarrow \mu^+ \mu^-)$ which are correlated to $\text{BR}(B_s \rightarrow \mu^+ \mu^-)$, will play a crucial role in shaping the parameter space of the MSSM-30. On the other hand, systematically constructed frameworks which can capture the flavor structure of the MSSM, like the one presented here, should be favored over simplified scenarios which cannot capture the rich flavor structure of the MSSM.

Acknowledgments

We would like to thank Janusz Rosiek for help and comments regarding SUSY_FLAVOR. L.V.S thanks R. Fleischer for comments regarding $\text{BR}(B_s \rightarrow \mu^+ \mu^-)$ and the Abdus Salam International Center for Theoretical Physics, Italy, for support and hospitality during the last stages of this project. During an earlier stage of this work, S.S.A. was funded at INFN, Sezione di Roma, under the European Research Council's Seventh Framework Programme (FP/2007-2013)/ERC Grant Agreement no. 279972, NPFlavour.

References

- [1] C. Bobeth, T. Ewerth, F. Kruger and J. Urban, Phys. Rev. D **64** (2001) 074014 doi:10.1103/PhysRevD.64.074014 [hep-ph/0104284].
- [2] C. Bobeth, T. Ewerth, F. Kruger and J. Urban, Phys. Rev. D **66** (2002) 074021 doi:10.1103/PhysRevD.66.074021 [hep-ph/0204225].
- [3] C. S. Huang, W. Liao and Q. S. Yan, Phys. Rev. D **59** (1999) 011701 doi:10.1103/PhysRevD.59.011701 [hep-ph/9803460].
- [4] C. Hamzaoui, M. Pospelov and M. Toharia, Phys. Rev. D **59** (1999) 095005 doi:10.1103/PhysRevD.59.095005 [hep-ph/9807350].
- [5] S. R. Choudhury and N. Gaur, Phys. Lett. B **451** (1999) 86 doi:10.1016/S0370-2693(99)00203-8 [hep-ph/9810307].
- [6] K. S. Babu and C. F. Kolda, Phys. Rev. Lett. **84** (2000) 228 doi:10.1103/PhysRevLett.84.228 [hep-ph/9909476].

[7] C. S. Huang, W. Liao, Q. S. Yan and S. H. Zhu, Phys. Rev. D **63** (2001) 114021 Erratum: [Phys. Rev. D **64** (2001) 059902] doi:10.1103/PhysRevD.64.059902, 10.1103/PhysRevD.63.114021 [hep-ph/0006250].

[8] S. S. AbdusSalam, B. C. Allanach, F. Quevedo, F. Feroz and M. Hobson, Phys. Rev. D **81** (2010) 095012 doi:10.1103/PhysRevD.81.095012 [arXiv:0904.2548 [hep-ph]].

[9] A. Arbey, M. Battaglia, F. Mahmoudi and D. Martnez Santos, Phys. Rev. D **87** (2013) no.3, 035026 doi:10.1103/PhysRevD.87.035026 [arXiv:1212.4887 [hep-ph]].

[10] W. Altmannshofer, C. Niehoff and D. M. Straub, JHEP **1705** (2017) 076 doi:10.1007/JHEP05(2017)076 [arXiv:1702.05498 [hep-ph]].

[11] T. Aaltonen *et al.* [CDF Collaboration], Phys. Rev. Lett. **107** (2011) 191801 [Phys. Rev. Lett. **107** (2011) 239903] Addendum: [Phys. Rev. Lett. **107** (2011) no.23, 239903] doi:10.1103/PhysRevLett.107.191801, 10.1103/PhysRevLett.107.239903 [arXiv:1107.2304 [hep-ex]].

[12] V. M. Abazov *et al.* [D0 Collaboration], Phys. Lett. B **693** (2010) 539 doi:10.1016/j.physletb.2010.09.024 [arXiv:1006.3469 [hep-ex]].

[13] R. Aaij *et al.* [LHCb Collaboration], Phys. Rev. Lett. **108** (2012) 231801 doi:10.1103/PhysRevLett.108.231801 [arXiv:1203.4493 [hep-ex]].

[14] S. Chatrchyan *et al.* [CMS Collaboration], JHEP **1204** (2012) 033 doi:10.1007/JHEP04(2012)033 [arXiv:1203.3976 [hep-ex]].

[15] G. Aad *et al.* [ATLAS Collaboration], Phys. Lett. B **713** (2012) 387 doi:10.1016/j.physletb.2012.06.013 [arXiv:1204.0735 [hep-ex]].

[16] R. Aaij *et al.* [LHCb Collaboration], Phys. Rev. Lett. **110** (2013) no.2, 021801 doi:10.1103/PhysRevLett.110.021801 [arXiv:1211.2674 [hep-ex]].

[17] V. Khachatryan *et al.* [CMS and LHCb Collaborations], Nature **522** (2015) 68 doi:10.1038/nature14474 [arXiv:1411.4413 [hep-ex]].

[18] M. Mulder [LHCb Collaboration], arXiv:1705.03274 [hep-ex].

[19] R. Aaij *et al.* [LHCb Collaboration], Phys. Rev. Lett. **118**, no. 19, 191801 (2017) doi:10.1103/PhysRevLett.118.191801 [arXiv:1703.05747 [hep-ex]].

[20] G. Colangelo, E. Nikolidakis and C. Smith, Eur. Phys. J. C **59** (2009) 75 doi:10.1140/epjc/s10052-008-0796-y [arXiv:0807.0801 [hep-ph]].

[21] S. S. AbdusSalam, C. P. Burgess and F. Quevedo, JHEP **1502** (2015) 073 doi:10.1007/JHEP02(2015)073 [arXiv:1411.1663 [hep-ph]].

[22] A. Dedes, H. K. Dreiner and U. Nierste, Phys. Rev. Lett. **87** (2001) 251804 doi:10.1103/PhysRevLett.87.251804 [hep-ph/0108037].

[23] J. R. Ellis, K. A. Olive and V. C. Spanos, Phys. Lett. B **624** (2005) 47 doi:10.1016/j.physletb.2005.07.066 [hep-ph/0504196].

[24] S. Heinemeyer, X. Miao, S. Su and G. Weiglein, JHEP **0808** (2008) 087 doi:10.1088/1126-6708/2008/08/087 [arXiv:0805.2359 [hep-ph]].

[25] A. K. Alok and S. K. Gupta, Eur. Phys. J. C **65** (2010) 491 doi:10.1140/epjc/s10052-009-1163-3 [arXiv:0904.1878 [hep-ph]].

[26] F. Mahmoudi, S. Neshatpour and J. Orloff, JHEP **1208** (2012) 092 doi:10.1007/JHEP08(2012)092 [arXiv:1205.1845 [hep-ph]].

[27] O. Buchmueller *et al.*, Eur. Phys. J. C **72** (2012) 2243 doi:10.1140/epjc/s10052-012-2243-3 [arXiv:1207.7315 [hep-ph]].

[28] F. U. Bernlochner *et al.* [GAMBIT Collaboration], arXiv:1705.07933 [hep-ph].

[29] A. Djouadi *et al.* [MSSM Working Group], hep-ph/9901246.

[30] K. Kadota, G. Kane, J. Kersten and L. Velasco-Sevilla, Eur. Phys. J. C **72**, 2004 (2012) doi:10.1140/epjc/s10052-012-2004-3 [arXiv:1107.3105 [hep-ph]].

[31] J. Ellis, K. Olive and L. Velasco-Sevilla, Eur. Phys. J. C **76**, no. 10, 562 (2016) doi:10.1140/epjc/s10052-016-4398-9 [arXiv:1605.01398 [hep-ph]].

[32] Z. Poh and S. Raby, Phys. Rev. D **92**, no. 1, 015017 (2015) doi:10.1103/PhysRevD.92.015017 [arXiv:1505.00264 [hep-ph]].

[33] S. S. AbdusSalam, AIP Conf. Proc. **1078** (2009) 297 doi:10.1063/1.3051939 [arXiv:0809.0284 [hep-ph]].

[34] S. S. AbdusSalam and F. Quevedo, Phys. Lett. B **700** (2011) 343 doi:10.1016/j.physletb.2011.02.065 [arXiv:1009.4308 [hep-ph]].

[35] S. S. AbdusSalam, Phys. Lett. B **705** (2011) 331 doi:10.1016/j.physletb.2011.10.023 [arXiv:1106.2317 [hep-ph]].

[36] S. S. AbdusSalam *et al.*, Eur. Phys. J. C **71** (2011) 1835 doi:10.1140/epjc/s10052-011-1835-7 [arXiv:1109.3859 [hep-ph]].

[37] S. S. AbdusSalam and D. Choudhury, Universal J. Phys. Appl. **2** (2014) no.3, 155 doi:10.13189/ujpa.2014.020303 [arXiv:1210.3331 [hep-ph]].

[38] S. S. AbdusSalam, Phys. Rev. D **87** (2013) no.11, 115012 doi:10.1103/PhysRevD.87.115012 [arXiv:1211.0999 [hep-ph]].

[39] S. S. AbdusSalam, Int. J. Mod. Phys. A **29** (2014) no.27, 1450160 doi:10.1142/S0217751X14501607 [arXiv:1312.7830 [hep-ph]].

[40] S. S. AbdusSalam and L. Velasco-Sevilla, Phys. Rev. D **94** (2016) no.3, 035026 doi:10.1103/PhysRevD.94.035026 [arXiv:1506.02499 [hep-ph]].

[41] G. Belanger, F. Boudjema, A. Pukhov and A. Semenov, Comput. Phys. Commun. **180** (2009) 747 [arXiv:0803.2360 [hep-ph]].

[42] P. Z. Skands, B. C. Allanach, H. Baer, C. Balazs, G. Belanger, F. Boudjema, A. Djouadi and R. Godbole *et al.*, JHEP **0407** (2004) 036 [hep-ph/0311123].

[43] B. C. Allanach, C. Balazs, G. Belanger, M. Bernhardt, F. Boudjema, D. Choudhury, K. Desch and U. Ellwanger *et al.*, Comput. Phys. Commun. **180** (2009) 8 [arXiv:0801.0045 [hep-ph]].

[44] W. Porod and F. Staub, Comput. Phys. Commun. **183** (2012) 2458 [arXiv:1104.1573 [hep-ph]].

[45] A. Crivellin, J. Rosiek, P. H. Chankowski, A. Dedes, S. Jaeger and P. Tanedo, Comput. Phys. Commun. **184** (2013) 1004 doi:10.1016/j.cpc.2012.11.007 [arXiv:1203.5023 [hep-ph]].

[46] P. H. Chankowski and L. Slawianowska, Phys. Rev. D **63** (2001) 054012 doi:10.1103/PhysRevD.63.054012 [hep-ph/0008046].

[47] H. E. Logan and U. Nierste, Nucl. Phys. B **586** (2000) 39 doi:10.1016/S0550-3213(00)00417-X [hep-ph/0004139].

[48] A. Dedes, J. Rosiek and P. Tanedo, Phys. Rev. D **79** (2009) 055006 doi:10.1103/PhysRevD.79.055006 [arXiv:0812.4320 [hep-ph]].

[49] G. Raven [LHCb Collaboration], arXiv:1212.4140 [hep-ex].

[50] S. Chatrchyan *et al.* [CMS Collaboration], Phys. Rev. Lett. **111**, 101804 (2013) doi:10.1103/PhysRevLett.111.101804 [arXiv:1307.5025 [hep-ex]].

[51] A. J. Buras, R. Fleischer, J. Girkbach and R. Knegjens, JHEP **1307** (2013) 77 doi:10.1007/JHEP07(2013)077 [arXiv:1303.3820 [hep-ph]].

[52] C. Bobeth, M. Gorbahn, T. Hermann, M. Misiak, E. Stamou and M. Steinhauser, Phys. Rev. Lett. **112**, 101801 (2014) doi:10.1103/PhysRevLett.112.101801 [arXiv:1311.0903 [hep-ph]].